

PBBFMM3D: a parallel black-box algorithm for kernel matrix-vector multiplication

Ruoxi Wang^a, Chao Chen^a, Jonghyun Lee^b, Eric Darve^{a,c}

^a*Institute for Computational and Mathematical Engineering, Stanford University*

^b*Water Resources Research Center, Department of Civil and Environmental Engineering, University of Hawaii*

^c*Department of Mechanical Engineering, Stanford University*

Abstract

We introduce PBBFMM3D, a parallel black-box method for computing kernel matrix-vector multiplication, where the underlying kernel is a non-oscillatory function in three dimensions. While a naive method requires $\mathcal{O}(N^2)$ computation, PBBFMM3D reduces the cost to $\mathcal{O}(N)$ work. In particular, our algorithm requires only the ability to evaluate the kernel function, and is thus a black-box method. To further accelerate the computation on shared-memory machines, a parallel algorithm is presented and implemented using **OpenMP**, which achieved at most $19\times$ speedup on 32 cores in our numerical experiments. A real-world application in geostatistics is also presented, where PBBFMM3D is used in computing the truncated eigen-decomposition (a.k.a., principle component analysis) of a covariance matrix (a.k.a., graph Laplacian).

Keywords: kernel matrix-vector multiplication, covariance matrix, fast multipole method, shared-memory parallelism

1. Introduction

We consider the problem of computing kernel matrix-vector product, where the kernel function is **non-oscillatory**, **translation invariant** and sufficiently **smooth** away from the origin (NOTIS). The problem can be formu-

Email addresses: ruoxi.rw@gmail.com (Ruoxi Wang), chenchao.nk@gmail.com (Chao Chen), jonghyun.harry.lee@hawaii.edu (Jonghyun Lee), darve@stanford.edu (Eric Darve)

lated mathematically as evaluating

$$\phi_i = \sum_{j=1}^N \mathcal{K}(\mathbf{x}_i, \mathbf{y}_j) \sigma_j, \quad i = 1, \dots, N \quad (1)$$

where $\{\mathbf{x}_i\}_{i=1}^N$ and $\{\mathbf{y}_i\}_{i=1}^N$ are the target and the source data points in a cubical domain, respectively, σ_j is the weight associated with \mathbf{y}_j , and $\mathcal{K}(\mathbf{x}_i, \mathbf{y}_j) = \mathcal{K}(\mathbf{x}_i - \mathbf{y}_j)$ is a NOTIS function, such as $1/\|\mathbf{x}_i - \mathbf{y}_j\|$, $\exp(-\|\mathbf{x}_i - \mathbf{y}_j\|^2)$. In many applications, the two sets of points $\{\mathbf{x}_i\}_{i=1}^N$ and $\{\mathbf{y}_i\}_{i=1}^N$ may overlap. Algebraically, Eq. (1) can be written as the following matrix-vector multiplication:

$$\boldsymbol{\phi} = \mathbf{K}\boldsymbol{\sigma}, \quad (2)$$

where $\boldsymbol{\sigma} = [\sigma_1, \dots, \sigma_N]^T$ and $\boldsymbol{\phi} = [\phi_1, \dots, \phi_N]^T$ are two vectors, and \mathbf{K} is an N -by- N matrix with $\mathbf{K}_{ij} = \mathcal{K}(\mathbf{x}_i, \mathbf{y}_j)$. Such type of computation arises in many science and engineering fields, such as kernel methods in statistical learning and machine learning [1, 2], data assimilation methods in geosciences [3, 4], particle simulations and boundary integral/element methods in computational physics [5, 6, 7], dislocation dynamics simulations in material science [8, 9, 10, 11] and etc. To compute $\boldsymbol{\phi}$ in Eq. (2), a naive direct evaluation requires $\mathcal{O}(N^2)$ computation, which is prohibitive when N is large.

1.1. Previous work

One special but important instance of Eq. (1) is when the data points $\{\mathbf{x}_i\}_{i=1}^N$ and $\{\mathbf{y}_i\}_{i=1}^N$ lie on a regular grid. Then the fast Fourier Transform (FFT) can be applied with $\mathcal{O}(N \log(N))$ work, and Eq. (1) is evaluated exactly (up to round-off errors). Although extensions of the FFT to non-uniform data distributions exists [12, 13], they are not efficient for highly irregular distributions in three dimensions (3D).

The fast multipole method (FMM) is a general framework that has been successfully applied for non-uniform data distributions. The way the FMM works is to partition the problem domain hierarchically into subdomains of different scales, and then Eq. (1) is evaluated using the multiscale decomposition, where the calculation is computed exactly for adjacent subdomains at the finest scale and is approximated via separation of variables (low-rank approximation of submatrices in \mathbf{K}) otherwise. While the FMM has been derived for specific kernels that appear frequently in computational physics [5, 14, 15, 16, 17], the derivation may be tedious, difficult or even impossible for a complicated kernel function that may not even have a closed analytic formula.

Therefore, black-box/kernel-independent FMM have been developed that require only the evaluation of the kernel function. We classify these methods into two groups. The first consists of methods that approximate the kernel function (away from the origin) with polynomials such as Legendre polynomials and Chebyshev polynomials [18, 19, 20, 11]. The other group consists of methods that compute the so-called equivalent densities or the so-called skeletons for every subdomain to efficiently represent the contained source points and their weights [21, 22, 23, 24]. Theoretically, this approach is justified by the potential theory for kernel functions that are fundamental solutions of non-oscillatory elliptic partial differential equations.

1.2. Contributions

In this paper, we present a parallel implementation of the black-box method in [20, 11] for evaluating Eq. (1) using $\mathcal{O}(N)$ memory and computation. The key idea is using Lagrange interpolation to construct approximations of the kernel function $\mathcal{K}(\mathbf{x}, \mathbf{y})$ when \mathbf{x} and \mathbf{y} are distant. Unlike fast algorithms that have been developed for specific kernel functions, our method applies to a wide range of functions. Success stories include applications of our method in dislocation dynamics simulations [11] and aquifer characterization [25], where no previous fast algorithm exists for the two kernel functions—the Green’s function in anisotropic elasticity and the isotropic exponential function. In particular, our method requires only a black-box routine to evaluate the kernel function, and thus can be integrated easily with other codes. For example, our package was used in an iso-geometric boundary element method to obtain a solver of $\mathcal{O}(N)$ complexity [7]. Other examples of using (an earlier version of) our code are in the elastic formulation of the displacement discontinuity method for the simulation of micro-seismicity [26, 27, 28].

To evaluate Eq. (1), our method follows the general FMM machinery as follows. First, the problem domain containing $\{\mathbf{x}_i\}_{i=1}^N$ and $\{\mathbf{y}_i\}_{i=1}^N$ is partitioned in a hierarchical fashion (see Fig. 1(a)), and the partitioning is associated with a tree data structure where every tree node represents a subdomain in the hierarchy. Second, a post-order traversal of the tree is performed, and the “multipole coefficients” associated with every tree node is computed as a compact representation of the source points and corresponding weights that the subdomain contains. This step is often called an upward pass. Third, at every level of the hierarchy, the “local coefficients” of every tree node is computed using the “multipole coefficients” of its *interaction list* (two nodes are in each other’s interaction list if their parents are adjacent but they are not; see Fig. 1(b)). Fourth, a pre-order traversal of the tree is performed to “accumulate” the local coefficients of all nodes to those at the leaf level.

This step is often called an downward pass. Finally, the contribution from adjacent subdomains are evaluated exactly for all leaf nodes. Technically speaking, multipole and local coefficients are terminologies used in the original FMM [5], here we stick to the same terms for their counterparts in our algorithm, which we will rigorously define in Section 2.3.

Our parallel algorithm is based on three basic observations of the above procedure: (1) the computation of multipole coefficients and local coefficients during the upward pass and the downward pass is embarrassingly parallel for tree nodes at the same level; (2) the computation of local coefficients is embarrassingly parallel for all nodes; and (3) the exact evaluation of the contribution from adjacent subdomains is embarrassingly parallel for all leaf nodes. Note that our implementation does not exploit task-level parallelism [29], which usually requires a well-designed runtime system, but our results show satisfactory parallel speedups on up to 32 cores on a shared-memory machine.

To summarize, we present PBBFMM3D—**parallel black-box FMM in 3D**—to compute the kernel matrix-vector multiplication in Eq. (1) for NOTIS kernels. The algorithm provably requires $\mathcal{O}(N)$ memory and work. Our parallel implementation is based on the `OpenMP` API [30] and targets shared-memory machines. The code is publicly available at

<https://github.com/ruoxi-wang/PBBFMM3D>

1.3. Outline

The rest of this paper is organized as follows. Section 2 describes the algorithm focusing on the data dependency and the parallelism. Section 3 describes the software architecture and the user interface. Section 4 presents numerical results on the accuracy, the sequential and parallel running time of PBBFMM3D with a real-world application. Section 5 draws the conclusion.

2. Parallel black-box algorithm

In this section, we present the black-box algorithm for evaluating Eq. (1). In particular, we focus on the data dependency and illustrate our parallel strategy. Although our code deals with 3D problems, we use 1D and 2D examples here for pictorial illustration.

2.1. Hierarchical domain decomposition

As with other multilevel methods, our method is based on a hierarchical decomposition of the problem domain in order to achieve linear complexity. Specifically, the 3D cubical spatial domain is split into eight subdomains

(divided in half in three coordinate directions) recursively until the number of data points in every subdomain is less than a prescribed constant. This hierarchical domain decomposition is naturally associated with a tree data structure \mathcal{T} (binary-tree in 1D, quadtree in 2D and octree in 3D), where the root stands for the entire domain, and the other nodes stand for subdomains at different levels in the hierarchy; see Fig. 1(a). For the rest of the paper, we use the terms subdomain and tree node interchangeably.

Note the hierarchical decomposition is generally non-uniform (\mathcal{T} is adaptive). But we choose to use a uniform-tree data structure in PBBFMM3D for the ease of parallel implementation, which is reasonably efficient as long as the point distribution is not extremely irregular. With a uniform tree, some leaf nodes may end up having few data points. In PBBFMM3D, empty nodes are skipped in the algorithm, and the overhead of using a uniform tree compared with an adaptive one is from processing nodes that have only a few points.

Given the tree \mathcal{T} , the *parent* $\mathcal{P}(\alpha)$ and the *children* $\mathcal{C}(\alpha)$ of a node α are naturally defined. We also define the neighbors $\mathcal{N}(\alpha)$ and the interaction list $\mathcal{I}(\alpha)$ of a node α as below; see Fig. 1(b) for an pictorial illustration.

Definition 2.1 (Neighbors and interaction list)

Given a hierarchical tree structure,

- $\mathcal{N}(\alpha)$: *the adjacent nodes (subdomains) of α at the same level in the hierarchy including α itself. The number of neighbors is generally 3^d , where d is the spatial dimension.*
- $\mathcal{I}(\alpha) = \mathcal{C}(\mathcal{N}(\mathcal{P}(\alpha)))/\mathcal{N}(\alpha)$: *the non-adjacent nodes (subdomains) at the same level in the hierarchy whose parents are neighbors of $\mathcal{P}(\alpha)$. The number of nodes in the interaction list is generally $6^d - 3^d$, where d is the spatial dimension.*

2.2. Separation of variables (low-rank approximation)

The key idea of our algorithm is to approximate the kernel function $\mathcal{K}(\mathbf{x}, \mathbf{y})$ through polynomial interpolation when the target point \mathbf{x} and the source point \mathbf{y} are distant. In this section, we focus on the situation where \mathbf{x} and \mathbf{y} are inside two non-adjacent subdomains, respectively. Technically speaking, \mathbf{x} and \mathbf{y} are *well-separated*. For the following discussion, we need a set of p interpolation nodes $\mathcal{S} = \{x_1^*, x_2^*, \dots, x_p^*\}$ on the real line. Then we can form interpolation nodes in 3D with tensor products:

$$\mathcal{S} \otimes \mathcal{S} \otimes \mathcal{S} = \{\mathbf{x}_i^* = (x_{i_1}^*, x_{i_2}^*, x_{i_3}^*), i_1, i_2, i_3 = 1, 2, \dots, p\},$$

where i and (i_1, i_2, i_3) are 1D-index and 3D-index of the $p \times p \times p$ grid, respectively, e.g., $i_1 = i \% p$, $i_2 = i \text{ mod } p$, and $i_3 = i \text{ mod } p^2$.

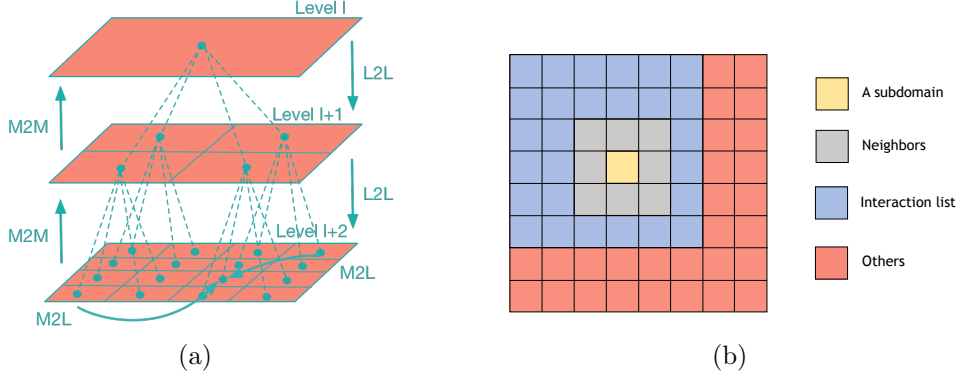


Figure 1: (a) hierarchical decomposition of the problem domain and the associated tree structure. The tree translation operators (M2M, M2L and L2L) are introduced in Section 2.3. (b) a subdomain α at the fourth level in the hierarchy, its neighbors $\mathcal{N}(\alpha)$ and its interaction list $\mathcal{I}(\alpha)$.

Definition 2.2 (Lagrange basis polynomials)

The p -th order Lagrange basis polynomials in 1D are

$$\ell_p(x_i^*, x) = \prod_{1 \leq k \leq p, k \neq i} \frac{x - x_k^*}{x_i^* - x_k^*}, \quad i = 1, 2, \dots, p.$$

The p -th order Lagrange basis polynomials in 3D are tensor products of the p -th order Lagrange basis polynomials in 1D:

$$L_p(\mathbf{x}_i^*, \mathbf{x}) = \ell_p(x_{i_1}^*, x_1) \ell_p(x_{i_2}^*, x_2) \ell_p(x_{i_3}^*, x_3), \quad i = 1, 2, \dots, p^3,$$

where $\mathbf{x} = (x_1, x_2, x_3) \in \mathbb{R}^3$, and $\mathbf{x}_i^* = (x_{i_1}^*, x_{i_2}^*, x_{i_3}^*) \in \mathcal{S} \otimes \mathcal{S} \otimes \mathcal{S}$.

Definition 2.3 (p -th order polynomial interpolant of $\mathcal{K}(\mathbf{x}, \mathbf{y})$)

Denote $\hat{\mathcal{K}}(\mathbf{x}, \mathbf{y})$ as the p -th order polynomial interpolant of $\mathcal{K}(\mathbf{x}, \mathbf{y})$, which is obtained through Lagrange interpolation on \mathbf{x} and \mathbf{y} , respectively (\mathbf{x} and \mathbf{y} are well-separated):

$$\begin{aligned} \mathcal{K}(\mathbf{x}, \mathbf{y}) &\approx \sum_{i=1}^{p^3} \mathcal{K}(\mathbf{x}_i^*, \mathbf{y}) L_p(\mathbf{x}_i^*, \mathbf{x}) \\ &\approx \sum_{i=1}^{p^3} \sum_{j=1}^{p^3} \mathcal{K}(\mathbf{x}_i^*, \mathbf{y}_j^*) L_p(\mathbf{x}_i^*, \mathbf{x}) L_p(\mathbf{y}_j^*, \mathbf{y}) = \hat{\mathcal{K}}(\mathbf{x}, \mathbf{y}), \end{aligned} \quad (3)$$

where $\mathbf{x}_i^*, \mathbf{y}_j^* \in \mathcal{S} \otimes \mathcal{S} \otimes \mathcal{S}$.

Observe that constructing the approximation $\hat{\mathcal{K}}(\mathbf{x}, \mathbf{y})$ requires only evaluations of the kernel function $\mathcal{K}(\mathbf{x}_i^*, \mathbf{y}_j^*)$.

The PBBFMM3D code offers two options for interpolation nodes, namely, Chebyshev nodes

$$\mathcal{S} = \left\{ \cos \left(\frac{2k-1}{2p} \pi \right), k = 1, 2, \dots, p \right\}$$

and equally spaced nodes

$$\mathcal{S} = \left\{ \frac{k-1}{p-1}, k = 1, 2, \dots, p \right\}.$$

With the Chebyshev nodes, the approximation in Eq. (3) is nearly optimal among polynomials of the same order. More importantly, the error decays as $\mathcal{O}(\rho^{-p})$ if the kernel function $K(\mathbf{x}, \mathbf{y})$ is analytic and bounded in the “Bernstein ellipse” of foci 1 and -1 with semimajor and semiminor axis lengths summing to ρ [31]. With equally spaced nodes, the matrix $\mathcal{K}(\mathbf{x}_i^*, \mathbf{y}_j^*)$ in Eq. (3) is a block-Toeplitz-Toeplitz-block matrix, which has a reduced memory footprint and can be applied in $\mathcal{O}(p^3 \log(p))$ time using the FFT [11]. Note the Lagrange interpolation of high degree over equally spaced nodes does not always converge, even for smooth functions, which is known as Runge’s phenomenon. In practice, we find low-order approximations sufficiently accurate in many applications. The scheme of Lagrange interpolation on uniform nodes can be stabilized by fitting a polynomial of degree $d < 2\sqrt{p}$ using least-squares.

2.3. Black-box FMM algorithm

To evaluate Eq. (1), our algorithm has the following four stages.

1. *Upward Pass.* A post-order traversal of \mathcal{T} is performed to compute the “multipole coefficients” of every subdomain, which encodes information of the source points and their weights contained in the subdomain. For every leaf node α in \mathcal{T} , the *particle-to-moment* (P2M) translation is executed:

$$\mathbf{M}_i^\alpha = \sum_{\mathbf{y}_j \in \alpha} L_p(\mathbf{y}_i^*, \mathbf{y}_j) \sigma_j, \quad i = 1, 2, \dots, p^3,$$

where \mathbf{y}_j and \mathbf{y}_i^* are the source points and interpolation nodes in α , respectively. For every non-leaf node α in \mathcal{T} , the *moment-to-moment* (M2M) translation is executed:

$$\mathbf{M}_i^\alpha = \sum_{\beta \in \mathcal{C}(\alpha)} \sum_{j=1}^{p^3} L_p(\mathbf{y}_i^*, \mathbf{y}_j^*) \mathbf{M}_j^\beta, \quad i = 1, 2, \dots, p^3,$$

where \mathbf{y}_i^* and \mathbf{y}_j^* are the interpolation nodes in α and β , respectively.

2. *Far-field interaction.* The “local coefficients” of every node is computed using the “multipole coefficients” of its interaction list. For every node α in \mathcal{T} , the *moment-to-local* (M2L) translation is executed:

$$\mathbf{F}_i^\alpha = \sum_{\beta \in \mathcal{I}(\alpha)} \sum_{j=1}^{p^3} \mathcal{K}(\mathbf{x}_i^*, \mathbf{y}_j^*) \mathbf{M}_j^\beta, \quad i = 1, 2, \dots, p^3,$$

where \mathbf{x}_i^* and \mathbf{y}_j^* are the interpolation nodes in α and β , respectively.

3. *Downward Pass.* A pre-order traversal of \mathcal{T} is performed to “accumulate” the “local coefficients” at leaf nodes. This is effectively a “transpose” of the upward pass. For every node α in \mathcal{T} , the *local-to-local* (L2L) translation is executed:

$$\mathbf{F}_i^\alpha += \sum_{j=1}^{p^3} \mathbf{F}_j^\beta L_p(\mathbf{x}_j^*, \mathbf{x}_i^*), \quad i = 1, 2, \dots, p^3,$$

where $\beta = \mathcal{P}(\alpha)$, \mathbf{x}_i^* and \mathbf{x}_j^* are the interpolation nodes in α and β , respectively. For every leaf node α in \mathcal{T} , the *local-to-particle* (L2P) translation is also executed:

$$\phi_i = \sum_{j=1}^{p^3} \mathbf{F}_j^\alpha L_p(\mathbf{x}_j^*, \mathbf{x}_i),$$

where \mathbf{x}_i and \mathbf{x}_j^* are the target points and interpolation nodes in α , respectively.

4. *Near-field interaction.* The contribution from neighbors is evaluated exactly. For every leaf node α , the *particle-to-particle* (P2P) translation is executed:

$$\phi_i += \sum_{\beta \in \mathcal{N}(\alpha)} \sum_{\mathbf{y}_j \in \beta} \mathcal{K}(\mathbf{x}_i, \mathbf{y}_j) \sigma_j,$$

where \mathbf{x}_i and \mathbf{y}_j are the target and the source points in α and β , respectively.

To summarize, the contribution from neighbors is calculated exactly; the contribution from the interaction list is approximated using the polynomial interpolant in Eq. (3); and the contribution from the remaining leaf nodes are approximated through coarser levels in the tree. A diagram illustrating the above process is shown in Fig. 2.

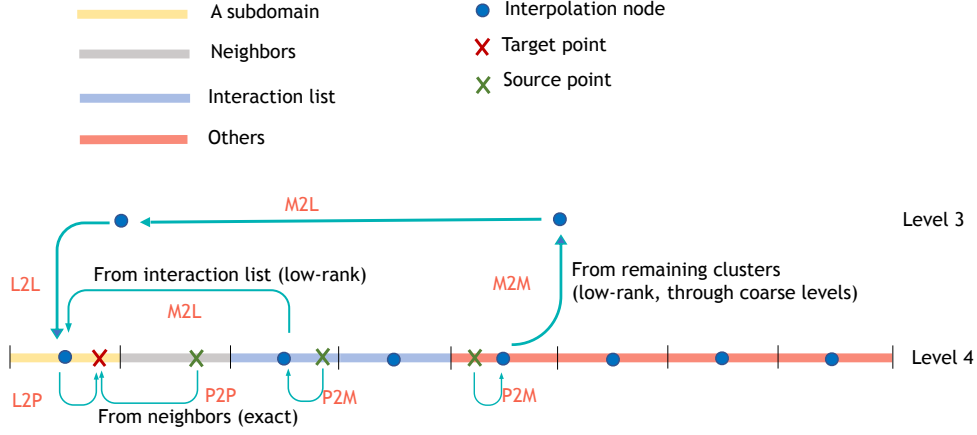


Figure 2: A one-dimensional FMM example with one target point and three source points. The calculation of Eq. (1) is divided into three parts: (1) P2P translation from the neighbor (grey), (2) P2M→M2L→L2P translations from the interaction list (blue), and (3) P2M→M2M→M2L→L2L→L2P translations from the remaining leaf nodes (red).

Below, we present a theorem for the computational cost and memory footprint of the above algorithm. Our primary focus is showing the complexity in terms of the number of points N , and thus we present the computational cost of one M2L translation as $\mathcal{O}(p^6)$, the cost of a naive matrix-vector product. For the same reason, we use an $\mathcal{O}(p^6)$ estimate for the storage of every M2L translation operator. Given the M2L translation is a bottleneck in the FMM, we implement acceleration techniques in PBBFMM3D, which is discussed in Section 2.5.

Theorem 2.1 (Computational cost and memory footprint)

The computational cost and memory footprint of the black-box FMM algorithm are both $\mathcal{O}(N)$.

Suppose every leaf node has at most n_0 points (typically $64 \sim 128$). The number of leaf nodes and the number of tree nodes are both $\mathcal{O}(N/n_0)$. In the above algorithm, every node requires constant amount of work (independent of N) at every stage:

1. *Upward Pass.* P2M: $\mathcal{O}(p^3 n_0)$ work for every leaf node. M2M: $\mathcal{O}(8p^4)$ work for every non-leaf node, where every non-leaf node has at most 8 children in 3D. Note the M2M is a 3D tensor-vector multiplication.
2. *Far-field interaction.* M2L: $\mathcal{O}(189p^6)$ work for every node, where the interaction list has at most $6^3 - 3^3 = 189$ nodes in 3D.

3. *Downward Pass.* L2L: $\mathcal{O}(p^4)$ work for every node. L2P: $\mathcal{O}(p^3 n_0)$ work for every leaf node. Note the L2L is a 3D tensor (transpose of the tensor in M2M)-vector multiplication.
4. *Near-field interaction.* P2P: $\mathcal{O}(27 n_0^2)$ work for every leaf node, where every node generally has at most $3^3 = 27$ neighbors in 3D.

Therefore, the computational complexity of the entire algorithm is $\mathcal{O}(N)$.

Regarding the memory footprint, every tree node stores p^3 “multipole coefficients” and p^3 “local coefficients”, which sums up to $\mathcal{O}(Np^3/n_0)$. Since the kernel function is translational invariant, we need to precompute only $7^3 - 3^3 = 316$ M2L translation operators at every level for the $\log(N)$ -level tree structure, which is $\mathcal{O}(316p^6 \log(N))$ memory in total. Therefore, the memory footprint is $\mathcal{O}(2p^3 N + 316p^6 \log(N))$.

2.4. Parallel algorithm

In this section, we analyze the parallelism in each of the four stages in the FMM algorithm, and we have implemented a parallel algorithm using the `OpenMP` API for shared-memory machines.

1. *Upward Pass.* As stated earlier, the upward pass is a post-order traversal of \mathcal{T} , so a parallel post-order tree traversal using `OpenMP` tasks [32] is implemented in `PBBFMM3D`.
2. *Far-field interaction.* The M2L translations are independent for all nodes. In addition, the translation typically requires the same amount of work for every node. Therefore, the `OpenMP` “parallel for” directive is employed on the loop over all nodes for M2L translations in `PBBFMM3D`.
3. *Downward Pass.* As stated earlier, the downward pass is a pre-order traversal of \mathcal{T} , so a parallel pre-order tree traversal using `OpenMP` tasks [32] is implemented in `PBBFMM3D`.
4. *Near-field interaction.* The P2P translations are independent for all leaf nodes. However, the translations between pairs of neighbors are work-heterogeneous due to the non-uniform distribution of the target and the source points. In `PBBFMM3D`, the `OpenMP` “parallel for” directive is employed on the loop over all leaf nodes for P2P translations, and different scheduling policies can be used based on any prior knowledge of the point distribution.

Algorithm 1 shows the pseudocode of the above parallel algorithm. A common alternative to the parallel tree traversal using `OpenMP` task is a level-by-level traversal with the `OpenMP` “parallel for” directive on the loop over

all nodes at the same level. Although the P2M and the L2P translations are work-heterogeneous, the efficiency of the alternative approach may still be reasonable since the upward pass and the downward pass are usually not the bottleneck.

Algorithm 1 Black-box FMM algorithm, where subroutines are shown in Algorithm 2 (ignoring the “pragma” lines leads to the serial algorithm)

```

1: # pragma omp parallel
2: # pragma omp single
3: UPWARD_PASS(root of  $\mathcal{T}$ )
4: FAR_FIELD_INTERACTION()
5: # pragma omp parallel
6: # pragma omp single
7: DOWNWARD_PASS(root of  $\mathcal{T}$ )
8: NEAR_FIELD_INTERACTION()

```

Here our parallel algorithm focuses on parallelizing each stage of the FMM algorithm, and haven’t exploit the concurrency across different stages. In principle, the near-field interaction stage does not depend on the others except for updating the results. So the work-heterogeneous P2P translations can be prioritized. Furthermore, notice the M2L translation of a node can happen as soon as its “multipole coefficients” have been computed. However, implementing these ideas for high performance would require a task-based runtime system, for which we refer interested readers to [29, 33].

2.5. Acceleration techniques

Since the far-field interaction and the near-field interaction usually dominate the entire computation, we introduce the acceleration techniques used in PBBFMM3D.

Homogeneous kernel. A kernel function is homogeneous if

$$\mathcal{K}(\alpha \mathbf{x}, \alpha \mathbf{y}) = \alpha^m \mathcal{K}(\mathbf{x}, \mathbf{y}),$$

for $\alpha \neq 0$ and m is typically an integer. For example, $\mathcal{K}(\mathbf{x}, \mathbf{y}) = 1/\|\mathbf{x} - \mathbf{y}\|$ is a homogeneous kernel function of degree -1. Since the interpolation grids are fixed relative to the problem domain, the M2L translation operators of different levels differ only by a scaling constant. Hence, we store these operators for only the leaf level.

Algorithm 2 Subroutines in the FMM algorithm

```
1: function UPWARD_PASS(node  $\alpha$ )
2:   for all node  $\beta \in \mathcal{C}(\alpha)$  do
3:     # pragma omp task
4:     UPWARD_PASS( $\beta$ )
5:   end for
6:   # pragma omp taskwait
7:   if  $\alpha$  is a leaf node then
8:     P2M translation
9:   else
10:    M2M translation
11:   end if
12: end function
13:
14: function FAR_FIELD_INTERACTION()
15:   # pragma omp parallel for
16:   for all node  $\alpha$  in  $\mathcal{T}$  do
17:     M2L translation
18:   end for
19: end function
20:
21: function DOWNWARD_PASS(node  $\alpha$ )
22:   if  $\alpha$  is a leaf node then
23:     L2P translation
24:   else
25:     L2L translation
26:   end if
27:   for all node  $\beta \in \mathcal{C}(\alpha)$  do
28:     # pragma omp task
29:     DOWNWARD_PASS( $\beta$ )
30:   end for
31: end function
32:
33: function NEAR_FIELD_INTERACTION()
34:   # pragma omp parallel for reduction(+:  $\phi$ )
35:   for all leaf node  $\alpha$  in  $\mathcal{T}$  do
36:     P2P translation
37:   end for
38: end function
```

Symmetry and skew-symmetry. A kernel function is symmetric if

$$\mathcal{K}(\mathbf{x}, \mathbf{y}) = \mathcal{K}(\mathbf{y}, \mathbf{x}),$$

and is skew-symmetric if

$$\mathcal{K}(\mathbf{x}, \mathbf{y}) = -\mathcal{K}(\mathbf{y}, \mathbf{x}).$$

In many applications, the source $\{\mathbf{x}_i\}_{i=1}^N$ and the target $\{\mathbf{y}_i\}_{i=1}^N$ are the same set of points. Therefore, the kernel matrix \mathbf{K} becomes symmetric or skew-symmetric if the kernel function is such. This implies only one of the two P2P/M2L translation operators needs be stored between a pair of tree nodes that are either neighbors or in each other's interaction list.

Fast M2L translation. Recall the definition of an M2L translation operator $\mathcal{K}(\mathbf{x}^*, \mathbf{y}^*)$ in Eq. (3), where \mathbf{x}^* and \mathbf{y}^* are interpolation grids in a pair of tree nodes that are in each other's interaction list. In PBBFMM3D, there are two options for the interpolation grids: Chebyshev nodes or equally spaced nodes. With Chebyshev nodes, an SVD-based compression of the M2L operator is employed following the approach in [20] since the translation operator is observed to be numerically low rank. With equally spaced nodes, the M2L operator is a block-Toeplitz-Toeplitz-block matrix [11], where the p^3 -by- p^3 matrix has only $(2p - 1)^3$ unique entries and can be applied to a vector in $\mathcal{O}(p^3 \log(p))$ time using the FFT.

Multiple right-hand-sides. In some applications, Eq. (1) needs to be evaluated with multiple weight vectors associated with the same set of source points. In PBBFMM3D, all weight vectors are grouped into a matrix as the input of the FMM algorithm, which allows using cache-friendly BLAS3 operations in our algorithm.

3. Software description.

In this section, we briefly discuss the software architecture of PBBFMM3D focusing on the black-box feature of the algorithm and the C++ and Python interfaces. More details can be found in the documentation at <https://github.com/ruoxi-wang/PBBFMM3D>. The code is written in C++ with the OpenMP API, and requires some standard linear algebra libraries including the BLAS¹, the LAPACK² and the FFTW3 library³. The Boost Python Library⁴ is required for using the Python interface.

¹<http://www.netlib.org/blas/>

²<http://www.netlib.org/lapack/>

³<http://www.fftw.org/>

⁴https://www.boost.org/doc/libs/1_70_0/libs/python/doc/html/index.html

The PBBFMM3D has the following three main classes as shown in Fig. 3.

- Class **H2_3D_Tree** sets parameters and creates the hierarchical partitioning of the problem domain. The parameters include (1) “**Domain size**”: side length of a cubical problem domain, (2) “**Tree level**”: the number of levels in the hierarchical partitioning, (3) “**Interpolation type**”: Chebyshev nodes or equally spaced nodes, (4) “**Interpolation order**”: the number of interpolation nodes used in Eq. (3), (5) “**SVD truncation error**”: error from the compression of the M2L translation operators, which is by default the prescribed accuracy of the entire computation. The two key member functions are the following. Function **PrecomputeM2L()** precomputes the M2L operators, and **BuildFMMHierarchy()** creates the hierarchical partitioning and builds the corresponding data structure.
- Class **H2_3D_Compute** stores the information regarding the source and the target points including (1) “**Target**”: position of target points $\{\mathbf{x}_i\}_{i=1}^N$, (2) “**Source**”: position of source points $\{\mathbf{y}_i\}_{i=1}^N$, (3) “**Weight**”: weights $\{\sigma_i\}_{i=1}^N$ associated with the source points, and (4) “**Number of weights**”: number of weights associated with every source point. The five key member functions include **FMMDistribute()**, which assigns the source and the target points to leaf cells in the tree, and four functions correspond to the four translation stages described in Section 2.
- Class **kernel_NAME** defines the kernel function. The member function **SetKernelProperty()** sets the homogeneous and the symmetric properties of the kernel function. The member function **EvaluateKernel()** takes two data points \mathbf{x} and \mathbf{y} and returns the value of $\mathcal{K}(\mathbf{x}, \mathbf{y})$.

C++ & Python interfaces. Listing 1 and 2 show the core lines of a basic example using the C++ interface and the Python interface, respectively. The example evaluates Eq. (1) with the standard Gaussian kernel. The first line creates an object of Class **kernel_Gaussian**, which implements the standard Gaussian function. The class inherits from class **H2_3D_Tree** and takes input parameters. The second line creates the hierarchical partitioning of the problem domain. The last line does the computation and stores results in the output variable.

```
// define kernel and set parameters for hierarchical partitioning
kernel_Gaussian tree(domain, level, IP_type, IP_order, SVD_err);
// partition
tree.buildFMMTree();
// FMM
H2_3D_Compute<kernel_Gaussian> compute(tree, target, source, weight, num_weight, result);
```

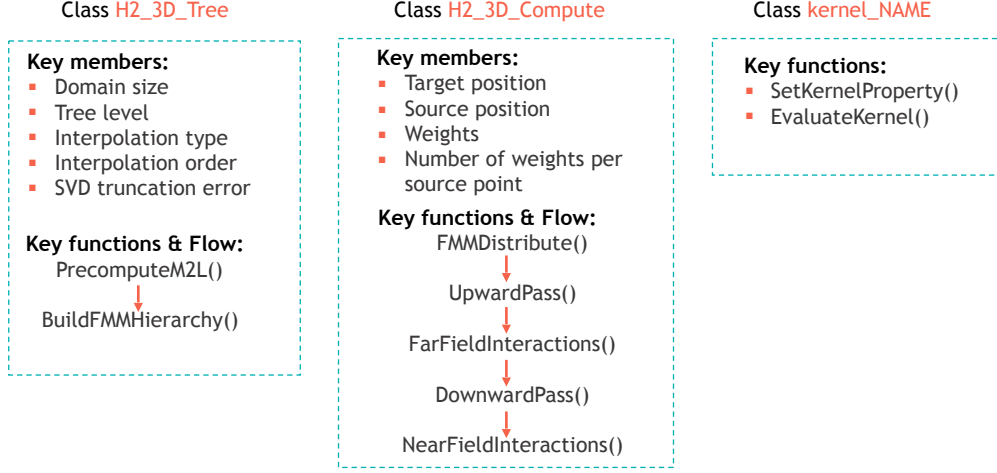


Figure 3: Three main classes in PBBFMM3D. The `H2_3D_Tree` class stores information regarding the hierarchical partitioning of the problem domain. The `H2_3D_Compute` class implements the FMM algorithm, and the `kernel_NAME` class describes the kernel function.

Listing 1: C++ interface. “`tree`” is an object of class `kernel_Gaussian`, which implements the standard Gaussian kernel. It also stores input parameters for the hierarchical partitioning. “`compute`” takes the positions of the target points, the source points, the associated weight vector(s), and the number of weight vectors. It evaluates Eq. (1) and outputs the results.

```
from FMMTree import *
from FMMCompute import *
# read/set inputs and parameters
...
# define kernel and set parameters for hierarchical partitioning
tree = kernel_Gaussian(domain, level, IP_type, IP_order, SVD_err)
# partition
tree.buildFMMTree()
# FMM
Compute(tree, target, source, weight, num_weight, result)
```

Listing 2: Python interface for the example in Listing 1.

Customized kernel. While some commonly used kernel functions are already implemented in PBBFMM3D, defining a new kernel function is straightforward as shown in Listing 3. It requires implementing only two methods as follows. The `EvaluateKernel()` method takes a pair of source and target points and returns the function value, and the `SetKernelProperty()` method tells

the homogeneous degree of the kernel and whether it is symmetric (see Section 2.5).

```
class myKernel: public H2_3D_Tree {
public:
    myKernel(double domain, int level, int IP_type, int IP_order, double SVD_err):
        H2_3D_Tree(domain, level, IP_type, IP_order, SVD_err) {};
    virtual void SetKernelProperty() {
        homogen = 0;
        symmetry = 1;
        kernelType = "exponential";
    }
    virtual double EvaluateKernel(const vector3 &target, const vector3 &source) {
        vector3 diff;
        diff.x = source.x - target.x;
        diff.y = source.y - target.y;
        diff.z = source.z - target.z;
        double r = std::sqrt(diff.x*diff.x+diff.y*diff.y+diff.z*diff.z);
        return std::exp(-r);
    }
};
```

Listing 3: Example of defining the $e^{-\|x-y\|}$ kernel. The function is symmetric but not homogeneous. Here, “vector3” is a structure of three floating point numbers representing coordinates in 3D.

4. Numerical Results

In this section, we present numerical experiments with PBBFMM3D to show the accuracy, the sequential running time and the parallel scalability. An real-world application in geostatistics is also presented, where PBBFMM3D was used to speed up the calculations with a covariance matrix. We focus on two particular kernel functions here: $1/\|\mathbf{x} - \mathbf{y}\|$ and $\exp(-\|\mathbf{x} - \mathbf{y}\|)$, where $1/\|\mathbf{x} - \mathbf{y}\|$, known as the Green’s function for the Laplace equation in 3D, is frequently used in computational physics, and $\exp(-\|\mathbf{x} - \mathbf{y}\|)$ is a popular choice as the covariance function for a Gaussian process.

All experiments were performed on a Linux server with 196 GB of RAM and the 36-core Intel Xeon CPU E5-2699 at 2.30GHz. The code was compiled with GCC 5.4.0, which implements version 4.0 of the OpenMP standard, and the code was linked with the Intel-MKL library⁵ of version 2018.3.222 and the FFTW3 library of version 3.3.6.

Parameters and notation.

- N : the number of source/target points, which are randomly generated using the uniform distribution in the unit cube.

⁵<https://software.intel.com/en-us/mkl>

- p : the order of interpolation, which determines the accuracy of our algorithm. Note the number of interpolation nodes is p^3 in Eq. (3) as a tensor product of p nodes in each dimension.
- **unif**: using equally spaced nodes in Eq. (3).
- **cheb**: using Chebyshev nodes in Eq. (3).
- **tree_level**: the number of levels of the hierarchical partitioning of the problem domain, which is chosen such that the average number of points in every leaf subdomain is about $64 \sim 128$.
- **SVD accuracy**: the compression accuracy of the M2L translation operator, which is chosen to be the same as the prescribed accuracy.
- r : notation of the Euclidean distance between a pair of source point \mathbf{x} and a target point \mathbf{y} , i.e., $\|\mathbf{x} - \mathbf{y}\|$.

4.1. Accuracy & sequential running time

In this section, we focus on two parameters N and p . First, we fix $N = 10^4$ and increase p to study the accuracy of PBBFMM3D. Then, we fix $p = 4$ and increase N to study the sequential running time. We refer to [11] for precomputation time and memory footprint when N is fixed and p increases.

Fig. 4 shows the (relative) errors of evaluating Eq. (1) as p increases (N is fixed), where the kernel functions are $\frac{1}{r}$ and e^{-r} , respectively. The error is defined as

$$\text{error} = \frac{\|\hat{K}\boldsymbol{\sigma} - K\boldsymbol{\sigma}\|_2}{\|K\boldsymbol{\sigma}\|_2},$$

where \hat{K} stands for the approximation that is implicitly defined by Eq. (3) in PBBFMM3D. Since both kernel functions are analytic away from the origin, errors of our interpolation using either the Chebyshev nodes or the uniform nodes decay exponentially fast as the number of nodes increases.

Fig. 5 shows the scaling of the sequential running time with respect to the number of points N . We see that the time increases linearly as N increases, as opposed to the quadratic increase of evaluating Eq. (1) directly.

4.2. Parallel scalability

In this section, we present the parallel running time of the PBBFMM3D code on up to 32 cores. We show results with respect to the kernel function $1/r$ and using the Chebyshev nodes in Eq. (3) with $p = 4$. Similar scalability results were obtained using the other kernel function e^{-r} or uniform nodes.

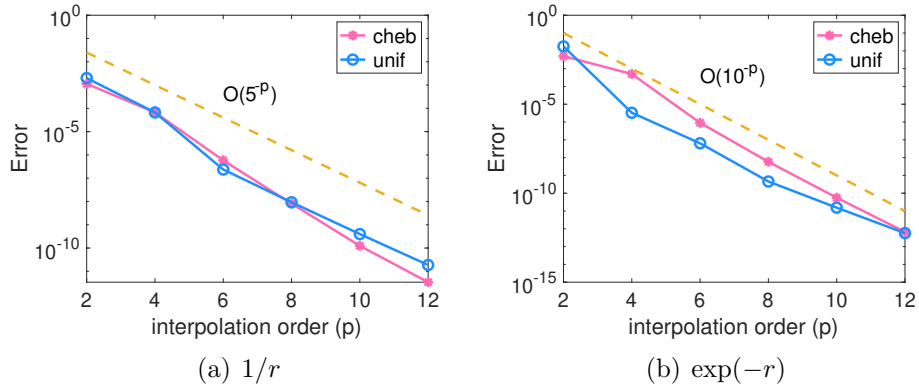


Figure 4: Relative error vs. interpolation order p , where $N = 10^4$ and `tree_level` = 5. Both `unif` and `cheb` lead to exponentially fast decay of errors.

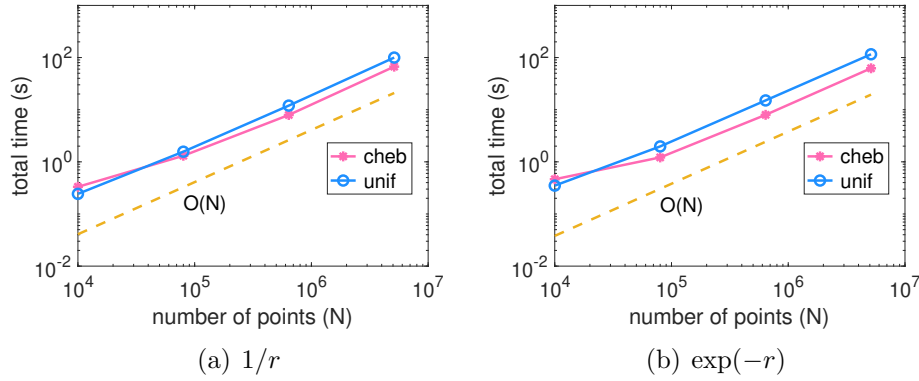


Figure 5: Sequential running time vs. number of points ($N = 10^4, 8 \times 10^4, 8^2 \times 10^4$, and $8^3 \times 10^4$). The interpolation order p is fixed at 4.

Table 1 reports the parallel running time for three increasing problem sizes on up to 32 cores. We see that the running time decreases as the number of cores increases. Specifically, for $N = 8^4 \times 10^4$, the runtime was accelerated by $19\times$ using 32 cores.

Table 1: Parallel running time for the kernel function $1/r$ and using Chebyshev interpolation nodes with $p = 4$. We set the number of tree levels to be 5, 6 and 7 for the three increasing problem sizes, and the errors are $2.10\text{e-}5$, $2.08\text{e-}5$, and $2.10\text{e-}5$, respectively.

N	Time (seconds)					
	1 core	2 cores	4 cores	8 cores	16 cores	32 cores
$8^2\text{e}+4$	5.74e+0	3.32e+0	1.83e+0	9.93e-1	5.84e-1	4.44e-1
$8^3\text{e}+4$	4.72e+1	2.58e+1	1.40e+1	7.87e+0	4.40e+0	3.49e+0
$8^4\text{e}+4$	4.04e+2	2.15e+2	1.14e+2	6.37e+1	3.72e+1	2.13e+1

Fig. 6(a) shows the strong scalability of PBBFMM3D, i.e., the running time using a sequence of increasing number of cores for a fixed problem size. We provided a breakdown of the running time into the four stages: upward pass, far-field interaction, downward pass, and near-field interaction. We see that the running time for all stages nearly halved as the number of cores doubled.

Fig. 6(b) shows the weak scalability of PBBFMM3D, i.e., the running time for a fixed problem size per core. So we increased the number of particles proportionally to the number of cores. As the figure shows, the time spent on each stage in the FMM only increased by a small amount when the problem size increased by $8\times$ (the number of cores also increased by $8\times$). The ideal runtime would stay unchanged due to the linear complexity of PBBFMM3D. Our implementation achieved an efficiency of 73% (serial time/parallel time).

4.3. Application in Gaussian processes

In this section, we present an application of using PBBFMM3D to accelerate computing a truncated eigen-decomposition of the covariance matrix that is used in Gaussian processes.

Gaussian random field (GRF) theory [34, 35] has been widely used in interpolation and estimation of spatially correlated unknowns. For example, estimating permeability of underground soil and rock is of critical interest for hydrogeologists and petroleum engineers [36, 37]. GRF requires a covariance matrix (a.k.a., graph Laplacian) as prior information of underlying unknown fields such as smoothness and uncertainty. Due to the large problem size encountered in practical applications, dimension reduction of the prior matrix through truncated eigenvalue decomposition has been investigated [38, 39, 40].

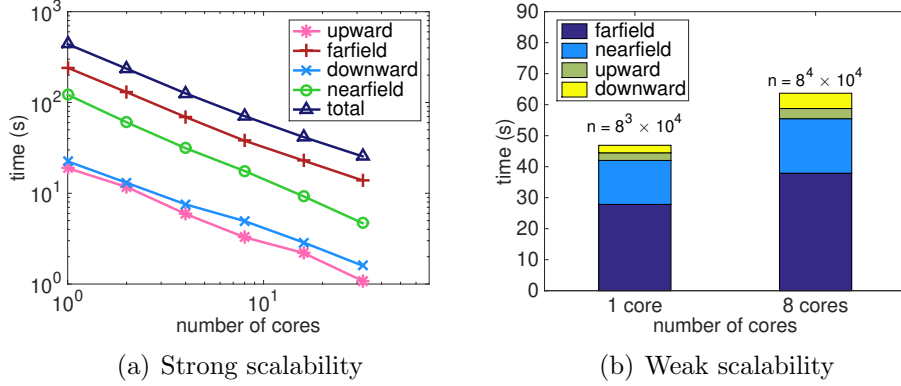


Figure 6: Parallel scalability and breakdown of the total time. Different colors stand for the total time and the four stages in the algorithm (see Section 2). Strong scalability results correspond to a fixed problem size of $N = 8^4 \times 10^4$, and weak scalability results correspond to a fixed problem size $8^3 \times 10^4$ per core.

We compute the truncated eigenvalue decomposition of dense covariance matrices using the randomized SVD (Algorithm 5.3 in [41]), which requires evaluating Eq. (1) k times (same target and source points but with k different weights) in order to calculate the top k eigenvalues and associated eigenvectors. Therefore, we can use PBBFMM3D to accelerate the calculation and total complexity would be $\mathcal{O}(Nk)$, where N is the number of data points.

Table 2 reports the speedup and the accuracy of using PBBFMM3D in the randSVD algorithm compared with using the exact evaluation. In these type of applications, we usually do not require a high accuracy such as $1e - 12$ or $1e - 10$, so we use the Chebyshev nodes with $p = 4$. Notice that forming the entire covariance matrix for $N = 64 \times 10^4$ requires more than 196 GB of RAM.

Lastly, we show the eigenvectors of the covariance matrix with the same kernel e^{-r} but with unstructured grids in the unit square [42]. As before, the eigenvectors are computed with the randSVD algorithm, where kernel matrix-vector product is calculated using PBBFMM3D with Chebyshev nodes ($p = 5$) on 32 cores.

5. Conclusions

We have introduced PBBFMM3D, a black-box algorithm/software for evaluating kernel matrix-vector multiplication on shared-memory machines. The target kernels are non-oscillatory translation invariant functions that are sufficiently smooth away from the origin. The user needs only provide a function routine that returns the kernel value given a source point and a target point,

Table 2: Comparison between using the exact evaluation and using the PBBFMM3D in computing the top-100 eigen-pairs of the covariance matrix via the randSVD algorithm on 32 cores. The covariance matrix \mathbf{K} corresponds to the one-dimensional Matérn kernel with smoothness $1/2$ (i.e., e^{-r}) and random uniformly distributed data points in a cube. In PBBFMM3D, the number of tree levels are 3, 4 and 5 for the three increasing problem sizes, and the Chebyshev nodes were used with $p = 4$. We measure the error by $\|\Lambda_{FMM} - \Lambda_{ext}\|_2 / \|\Lambda_{ext}\|_2$, where Λ_{ext} and Λ_{FMM} are the computed eigenvalues using the exact evaluation and the PBBFMM3D, respectively.

N	Time (seconds)		Speedup	Error
	PBBFMM3D	Exact		
10^4	1.30	19.1	$15\times$	1.6×10^{-4}
8×10^4	9.87	2139	$217\times$	2.8×10^{-5}
64×10^4	79.6	N/A	N/A	N/A

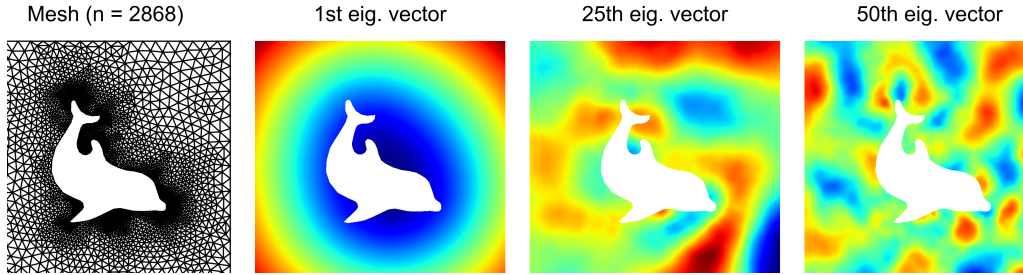


Figure 7: A unstructured mesh $N = 693,888$ from [42] and three eigenvectors of the covariance matrix with kernel e^{-r} . The eigenvectors are computed via the randSVD algorithm, where kernel matrix-vector product is calculated using PBBFMM3D with Chebyshev nodes $p = 5$ on 32 cores. The left most figure shows the (coarse) mesh with $N = 2868$ elements.

if the kernel function is not already implemented. (The user can also specify the degree of homogeneity and whether the kernel is symmetric or skew-symmetric to active specific optimizations.) Our algorithm requires $\mathcal{O}(N)$ memory and work, where N is the number of data points.

A parallel algorithm is presented in this paper and implemented using `OpenMP` for shared-memory machines. We have presented parallel scalability results on up to 32 cores and achieved at most $19\times$ speedup. We have also presented an application in accelerating the `randSVD` algorithm to compute the truncated eigen-decomposition of a covariance matrix used in geostatistics.

References

- [1] A. G. Gray, A. W. Moore, N-body problems in statistical learning, in: *Advances in neural information processing systems*, 2001, pp. 521–527.
- [2] T. Hofmann, B. Schölkopf, A. J. Smola, Kernel methods in machine learning, *The annals of statistics* (2008) 1171–1220.
- [3] S. Ambikasaran, A. K. Saibaba, E. F. Darve, P. K. Kitanidis, Fast algorithms for bayesian inversion, in: *Computational Challenges in the Geosciences*, Springer, 2013, pp. 101–142.
- [4] J. Y. Li, S. Ambikasaran, E. F. Darve, P. K. Kitanidis, A kalman filter powered by h2-matrices for quasi-continuous data assimilation problems, *Water Resources Research* 50 (5) (2014) 3734–3749.
- [5] L. Greengard, V. Rokhlin, A fast algorithm for particle simulations, *Journal of computational physics* 73 (2) (1987) 325–348.
- [6] L. Greengard, V. Rokhlin, A new version of the fast multipole method for the laplace equation in three dimensions, *Acta numerica* 6 (1997) 229–269.
- [7] R. Simpson, Z. Liu, Acceleration of isogeometric boundary element analysis through a black-box fast multipole method, *Engineering Analysis with Boundary Elements* 66 (2016) 168–182.
- [8] A. Arsenlis, W. Cai, M. Tang, M. Rhee, T. Oppelstrup, G. Hommes, T. G. Pierce, V. V. Bulatov, Enabling strain hardening simulations with dislocation dynamics, *Modelling and Simulation in Materials Science and Engineering* 15 (6) (2007) 553.

- [9] R. LeSar, J. Rickman, Multipole expansion of dislocation interactions: application to discrete dislocations, *Physical Review B* 65 (14) (2002) 144110.
- [10] D. Zhao, J. Huang, Y. Xiang, Fast multipole accelerated boundary integral equation method for evaluating the stress field associated with dislocations in a finite medium, *Communications in Computational Physics* 12 (1) (2012) 226–246.
- [11] C. Chen, S. Aubry, T. Oppelstrup, A. Arsenlis, E. Darve, Fast algorithms for evaluating the stress field of dislocation lines in anisotropic elastic media, *Modelling and Simulation in Materials Science and Engineering* (2018).
- [12] A. Dutt, V. Rokhlin, Fast fourier transforms for nonequispaced data, *SIAM Journal on Scientific computing* 14 (6) (1993) 1368–1393.
- [13] D. Ruiz-Antolin, A. Townsend, A nonuniform fast fourier transform based on low rank approximation, *SIAM Journal on Scientific Computing* 40 (1) (2018) A529–A547.
- [14] Y. Fu, K. J. Klimkowski, G. J. Rodin, E. Berger, J. C. Browne, J. K. Singer, R. A. Van De Geijn, K. S. Vemaganti, A fast solution method for three-dimensional many-particle problems of linear elasticity, *International Journal for Numerical Methods in Engineering* 42 (7) (1998) 1215–1229.
- [15] Y. Fu, G. J. Rodin, Fast solution method for three-dimensional Stokesian many-particle problems, *International Journal for Numerical Methods in Biomedical Engineering* 16 (2) (2000) 145–149.
- [16] L. F. Greengard, J. Huang, A new version of the fast multipole method for screened Coulomb interactions in three dimensions, *Journal of Computational Physics* 180 (2) (2002) 642–658.
- [17] K.-i. Yoshida, N. Nishimura, S. Kobayashi, Application of fast multipole Galerkin boundary integral equation method to elastostatic crack problems in 3d, *International Journal for Numerical Methods in Engineering* 50 (3) (2001) 525–547.
- [18] A. Dutt, M. Gu, V. Rokhlin, Fast algorithms for polynomial interpolation, integration, and differentiation, *SIAM Journal on Numerical Analysis* 33 (5) (1996) 1689–1711.

- [19] Z. Gimbutas, V. Rokhlin, A generalized fast multipole method for nonoscillatory kernels, *SIAM Journal on Scientific Computing* 24 (3) (2003) 796–817.
- [20] W. Fong, E. Darve, The black-box fast multipole method, *Journal of Computational Physics* 228 (23) (2009) 8712–8725.
- [21] L. Ying, G. Biros, D. Zorin, A kernel-independent adaptive fast multipole algorithm in two and three dimensions, *Journal of Computational Physics* 196 (2) (2004) 591–626.
- [22] P.-G. Martinsson, V. Rokhlin, An accelerated kernel-independent fast multipole method in one dimension, *SIAM Journal on Scientific Computing* 29 (3) (2007) 1160–1178.
- [23] D. Malhotra, G. Biros, Pvfmm: A parallel kernel independent fmm for particle and volume potentials, *Communications in Computational Physics* 18 (3) (2015) 808–830.
- [24] C. D. Yu, J. Levitt, S. Reiz, G. Biros, Geometry-oblivious fmm for compressing dense spd matrices, in: *Proceedings of the International Conference for High Performance Computing, Networking, Storage and Analysis*, ACM, 2017, p. 53.
- [25] J. Lee, A. Kokkinaki, P. K. Kitanidis, Fast large-scale joint inversion for deep aquifer characterization using pressure and heat tracer measurements, *Transport in Porous Media* 123 (2018) 533–543.
- [26] A. Verde, A. Ghassemi, et al., Efficient solution of large-scale displacement discontinuity problems using the fast multipole method, in: *47th US Rock Mechanics/Geomechanics Symposium*, American Rock Mechanics Association, 2013.
- [27] A. Verde, A. Ghassemi, Fast multipole displacement discontinuity method (fm-ddm) for geomechanics reservoir simulations, *International Journal for Numerical and Analytical Methods in Geomechanics* 39 (18) (2015) 1953–1974.
- [28] M. Farmahini-Farahani, A. Ghassemi, Simulation of micro-seismicity in response to injection/production in large-scale fracture networks using the fast multipole displacement discontinuity method (fmddm), *Engineering Analysis with Boundary Elements* 71 (2016) 179–189.

- [29] E. Agullo, B. Bramas, O. Coulaud, E. Darve, M. Messner, T. Takahashi, Task-based FMM for multicore architectures, *SIAM Journal on Scientific Computing* 36 (1) (2014) C66–C93.
- [30] OpenMP, <https://www.openmp.org/>.
- [31] L. N. Trefethen, *Approximation theory and approximation practice*, Siam, 2013.
- [32] Stanford university course: CME 213, http://web.stanford.edu/class/cme213/files/lectures/Lecture_05.pdf, accessed: 2019-11-30.
- [33] E. Agullo, B. Bramas, O. Coulaud, E. Darve, M. Messner, T. Takahashi, Task-based FMM for heterogeneous architectures, *Concurrency and Computation: Practice and Experience* 28 (9) (2016) 2608–2629.
- [34] C. E. Rasmussen, C. K. I. Williams, *Gaussian Processes for Machine Learning (Adaptive Computation and Machine Learning)*, The MIT Press, 2005.
- [35] M. L. Stein, *Interpolation of spatial data : some theory for kriging*, Springer series in statistics, Springer, New York, 1999.
- [36] P. K. Kitanidis, *Introduction to geostatistics: applications in hydrogeology*, Cambridge University Press, 1997.
- [37] D. S. Oliver, A. C. Reynolds, N. Liu, *Inverse theory for petroleum reservoir characterization and history matching*, Cambridge University Press, 2008.
- [38] T. Bui-Thanh, C. Burstedde, O. Ghattas, J. Martin, G. Stadler, L. C. Wilcox, Extreme-scale UQ for bayesian inverse problems governed by PDEs, in: *SC '12: Proceedings of the International Conference on High Performance Computing, Networking, Storage and Analysis*, 2012, pp. 1–11. doi:10.1109/SC.2012.56.
- [39] J. Lee, H. Yoon, P. K. Kitanidis, C. J. Werth, A. J. Valocchi, Scalable subsurface inverse modeling of huge data sets with an application to tracer concentration breakthrough data from magnetic resonance imaging, *Water Resources Research* 52 (7) (2016) 5213–5231.
- [40] A. K. Saibaba, J. Lee, P. K. Kitanidis, Randomized algorithms for generalized Hermitian eigenvalue problems with application to computing

- Karhunen–Loève expansion, *Numerical Linear Algebra with Applications* 23 (2) (2016) 314–339.
- [41] N. Halko, P.-G. Martinsson, J. A. Tropp, Finding structure with randomness: Probabilistic algorithms for constructing approximate matrix decompositions, *SIAM review* 53 (2) (2011) 217–288.
- [42] M. S. Alnæs, J. Blechta, J. Hake, A. Johansson, B. Kehlet, A. Logg, C. Richardson, J. Ring, M. E. Rognes, G. N. Wells, The FEniCS project version 1.5, *Archive of Numerical Software* 3 (100) (2015). doi:10.11588/ans.2015.100.20553.